A Wind-Induced Thermohaline Circulation Hysteresis and Millennial Variability Regimes

YOSEF ASHKENAZY

Solar Energy and Environmental Physics, BIDR, Ben-Gurion University, Midreshet Ben-Gurion, Israel

ELI TZIPERMAN

Department of Earth and Planetary Sciences, and Division of Engineering and Applied Sciences, Harvard University, Cambridge, Massachusetts

(Manuscript received 29 August 2006, in final form 12 December 2006)

ABSTRACT

The multiple equilibria of the thermohaline circulation (THC: used here in the sense of the meridional overturning circulation) as function of the surface freshwater flux has been studied intensively following a Stommel paper from 1961. It is shown here that multistability and hysteresis of the THC also exist when the wind stress amplitude is varied as a control parameter. Both the Massachusetts Institute of Technology ocean general circulation model (MITgcm) and a simple three-box model are used to study and explain different dynamical regimes of the THC and THC variability as a function of the wind stress amplitude. Starting with active winds and a thermally dominant thermohaline circulation state, the wind stress amplitude is slowly reduced to zero over a time period of ~40 000 yr (40 kyr) and then increased again to its initial value over another ~40 kyr. It is found that during the decreasing wind stress phase, the THC remains thermally dominant until very low wind stress amplitude at which pronounced Dansgaard–Oeschger-like THC relaxation oscillations are initiated. However, while the wind stress amplitude is increased, these relaxation oscillations are present up to significantly larger wind stress amplitude. The results of this study thus suggest that under the same wind stress amplitude, the THC can be either in a stable thermally dominant state or in a pronounced relaxation oscillations state. The simple box model analysis suggests that the observed hysteresis is due to the combination of the Stommel hysteresis and the Winton and Sarachik "deep decoupling" oscillations.

1. Introduction

The ocean, and the ocean meridional overturning circulation [here referred to as the thermohaline circulation (THC; Wunsch 2002)] in particular, are normally assumed to play an important role in climate dynamics, including both past climate variability such as the Heinrich (Heinrich 1988) and Dansgaard–Oeschger (DO) events (Dansgaard et al. 1984), and possible future climate change (Houghton et al. 2001). The multiple equilibria of the THC (Marotzke et al. 1988; Marotzke and Willebrand 1991; Stommel 1961), its different variability regimes due to nonlinear convective feedbacks (Cessi 1996; Lenderink and Haarsma 1994; Welander 1982; Winton 1993), interactions, and amplification by sea ice dynamics to result in significant rapid climate change (Gildor and Tziperman 2003; Kaspi et al. 2004) as well as due to linear advective dynamics (Griffies and Tziperman 1995), and its possible proximity to instability thresholds (Tziperman 1997; Tziperman et al. 1994) have been mostly studied as a function of the freshwater forcing (e.g., Bryan 1986; Gregory et al. 2003; Keeling 2002; Marotzke and Willebrand 1991; Nilsson and Walin 2001; Stouffer et al. 2006). However, wind stress is clearly a major driving force of the ocean circulation, driving both upper-ocean wind-driven circulation and western boundary currents, and a significant portion of the interior ocean mixing (Wunsch and Ferrari 2004). One therefore wonders what role the wind plays in the dynamics of the THC.

It is expected that the nonlinear ocean convection processes, large-scale advective THC dynamics, and the

Corresponding author address: Yosef Ashkenazy, Dept. of Solar Energy and Environmental Physics, The J. Blaustein Institute for Desert Research, Ben-Gurion University, Sede Boker Campus, 84990, Israel.
E-mail: ashkena@bgu.ac.il

DOI: 10.1175/JPO3124.1

wind-driven circulation are tightly coupled (Edwards et al. 1998; Hasumi and Suginohara 1999; Kohl 2005; Longworth et al. 2005; Oka et al. 2001; Pasquero and Tziperman 2004; Shaffer and Olsen 2001; Timmermann and Goosse 2004; Toggweiler and Samuels 1995; Tsujino and Suginohara 1999; Vallis 2000). The impact of the wind stress on the THC was studied using a simple box model by Stommel and Rooth (1968), followed by some more recent studies (Guan and Huang 2007; Longworth et al. 2005; MacMynowski and Tziperman 2006; Pasquero and Tziperman 2004). In addition, Timmermann and Goosse (2004) showed that gyration is essential for the existence of the THC of the Atlantic Ocean, while Hall and Stouffer (2001) indicated that abrupt climate events can result from the existence of winds in the North Atlantic.

The goal of this paper is to study the effect of wind-driven circulation on the THC, its stability, and variability regimes. Using an ocean general circulation model (OGCM) we find that the wind forcing, the nonlinear convectively induced DO-like variability, and the classic Stommel (1961) hysteresis are all strongly coupled in a very interesting manner. Specifically, we find that when decreasing the wind stress amplitude slowly (such that the model is always in equilibrium with the wind forcing), the model incurs different dynamical regimes, from a steady THC that is thermally dominant, to a nearly collapsed THC, to large DO-like relaxation oscillations as were previously observed (e.g., Kaspi 2002; Kaspi et al. 2004; Lenderink and Haarsma 1994; Rahmstorf and Ganopolski 1999; Vallis 2000; Wang and Mysak 2006; Winton 1993; Winton and Sarachik 1993). However, when increasing the wind stress slowly to its original value, these oscillations persist up to a much larger wind stress amplitude. Thus our two main novel findings are that (i) changes to the wind stress may change the dynamics of the THC, from stable THC to relaxation oscillations of THC and vice versa, and (ii) for the same wind stress amplitude two THC dynamics are possible, one with steady THC and one with strong relaxation oscillations of the THC.

We find that these seemingly surprising results have a simple and intuitive explanation. The winds control the amplitude of the wind-driven circulation, which in turns acts to horizontally mix the upper-ocean water between the midlatitudes and higher latitudes (Longworth et al. 2005; Oliver et al. 2005; Saltzman 2002; Stommel and Rooth 1968). This mixing increases the density of the high-latitude surface water by bringing low-latitude, high-salinity water that then cools and therefore becomes dense. This, in turn, affects the amplitude of the THC and can lead to the usual Stommel hysteresis that is normally found when changing the freshwater forcing. The weaker THC regime sometimes results in a deep ocean that is warmer and lighter, which then favors DO-like relaxation oscillations (Ganopolski and Rahmstorf 2001; Lenderink and Haarsma 1994; Welander 1982; Winton 1993; Winton and Sarachik 1993). Briefly, the hysteresis with respect to the wind stress is associated with Stommel (1961) freshwater flux hysteresis, while the relaxation oscillations observed for some wind stress amplitudes are associated with Winton and Sarachik (1993) relaxation oscillations.

The rest of the paper is organized as follows. We first describe the OGCM used in this study (section 2). We then present the results obtained by this OGCM (section 3). Next, a simple three-box model is presented to explain the OGCM results as a combination of Stommel and Winton mechanisms driven by the wind stress changes (section 4). We conclude in section 5.

2. Model configuration

a. The OGCM

We use the Massachusetts Institute of Technology general circulation model (MITgcm) (Adcroft et al. 2002; Marshall et al. 1997a,b). The MITgcm solves the primitive equations for the ocean, and is a free surface, finite volume, z-coordinate model with shaved bottom cells. It has several state-of-the-art subgrid parameterizations and boundary layer schemes. The model was applied to many problems over a wide range of spatial (from resolution of few meters to resolutions of several degrees) and temporal scales (Adcroft et al. 2002) and was used in the past with similar idealized configuration to the present study (Huang et al. 2003).

A box-geometry idealized model configuration is used. The depth is set uniformly to 4.5 km with 15 vertical levels of depth 20, 30, 40, 50, 60, 100, 150, 300, 400, 500, 550, 550, 550, 600, and 600 m. The horizontal double-hemisphere configuration, which seems preferable over a single hemisphere configuration for studying the THC (Dijkstra and Molemaker 1997), uses a resolution of 3° in latitude and longitude with 45 grid points in the meridional direction from 67.5°S to 67.5°N and 19 grid points in the zonal direction. The Redi (1982) and Gent and McWilliams (1990) parameterizations are used, together with the implicit vertical diffusion scheme of the MITgcm. Asynchronous integration (Bryan 1984) is used with a momentum time step of 1 h and a tracer time step of 10 h.

b. The surface forcing fields

We use mixed boundary conditions, that is, specified freshwater flux and restoring for surface temperature

(Bryan 1986). We verify below that our main results are not sensitive to the parameters involved in these oversimplified boundary conditions. The restoring temperature field, the evaporation minus precipitation field, and the wind stress field, are all zonally uniform and meridionally symmetric with respect to the equator. The evaporation minus precipitation field is similar to that of Wang et al. (1999). It is characterized by net evaporation in the subtropics and net precipitation elsewhere, broadly similar to the observations; the evaporation minus precipitation is maximal at 18°S and 18°N with value of 0.63 m yr^{-1} and is minimal at 60°S and 60°N with a value of -0.56 m yr^{-1} and secondary minimum at the equator with a value of -0.38 m yr^{-1}. Here $E - P$ is given by

$$\begin{aligned} E - P = {} & -0.0103(36.5491 - 2.388 \times 10^3 \sin^2\varphi \\ & + 1.963 \times 10^4 \sin^4\varphi - 6.556 \times 10^4 \sin^6\varphi \\ & + 1.083 \times 10^5 \sin^8\varphi - 8.703 \times 10^4 \sin^{10}\varphi \\ & + 2.703 \times 10^4 \sin^{12}\varphi), \end{aligned} \tag{1}$$

where φ is the latitude in radians and $E - P$ is in meters per year. In the following we use this evaporation minus precipitation field multiplied by a factor of either $f_{e-p} = 0.6$ or 0.7.

Easterly winds are specified in the low latitudes and westerlies in the high latitudes, resulting in a zonal wind stress field,

$$\tau_x = -0.1 \cos(\pi\varphi/\varphi_0)\ \mathrm{N\ m^{-2}}, \quad \tau_y = 0, \tag{2}$$

where $\varphi_0 = 66°\pi/180°$ is the latitude of the ocean's highest-latitude grid point.

The restoring temperature is set to

$$\mathrm{SST}_{\mathrm{restoring}} = -2 + 14.5[1 + \cos(\pi\varphi/\varphi_0)], \tag{3}$$

such that it is 27°C at the equator and -2°C at the highest latitudes. The restoring time scale is set to 24 days (the depth of the surface layer is 20 m), consistent with the estimate of Haney (1971). In some of the sensitivity tests below we also use restoring times of 12 and 48 days.

c. *Model spinup*

The simulation is initiated from a stratified ocean at rest with a uniform salinity (34.85 psu) and a specified temperature profile varying from 22°C at the top to 0°C at the bottom. A small temperature and salinity anomaly was introduced into the initial conditions in the northern high latitudes to break the meridional symmetry and force a northern sinking solution. The model was then run for 8000 years with the freshwater flux (1) using amplitude of $f_{e-p} = 0.6$, resulting in a steady-state maximum meridional overturning circulation of 17.6 Sv (Sv $\equiv 10^6$ m^3 s^{-1}). These spinup results are used as initial conditions for the numerical experiments described below.

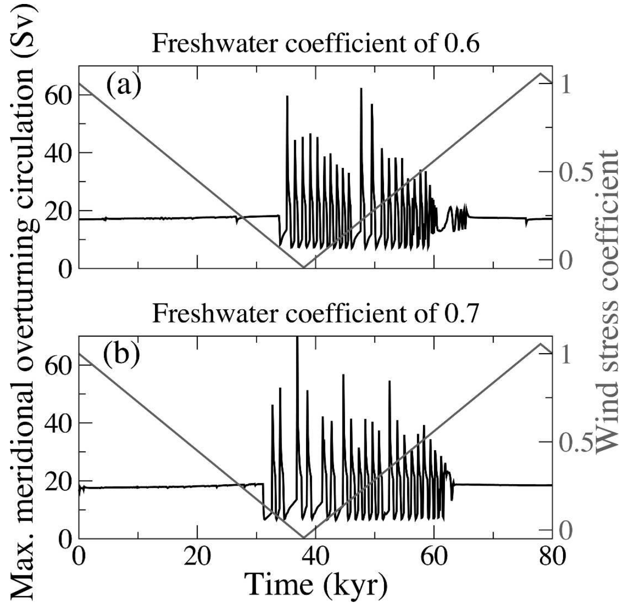

FIG. 1. Maximum meridional overturning circulation as a function of time for (a) freshwater coefficient $f_{e-p} = 0.6$ and (b) freshwater coefficient $f_{e-p} = 0.7$. The linear curve represents the wind stress coefficient. It is noticeable that, although the onset of the relaxation oscillations occurs for relatively low wind stress, the recovery to the initial overturning state occurs for much larger wind stress.

3. Results

Starting from the spinup solution, we run the model for 80 kyr where we decrease the zonal wind stress amplitude linearly in time over the first half of the simulation, and then increase it again to its original value over the second half of the simulation (Fig. 1). As the wind stress amplitude decreases, the meridional overturning circulation initially remains almost constant, with a slight increase in the maximum overturning circulation. After 34 kyr, relaxation oscillations of the meridional overturning circulation start.

The simulation of the entire period of slowly decreasing and increasing wind stress is shown in Fig. 1a, using the freshwater field of (1) with $f_{e-p} = 0.6$. The maximum meridional overturning circulation then remains almost constant, until the wind stress is very weak, when relaxation oscillations start. These oscillations persist at least for another 25 kyr and continue with smaller amplitude afterward for another 5 kyr. The

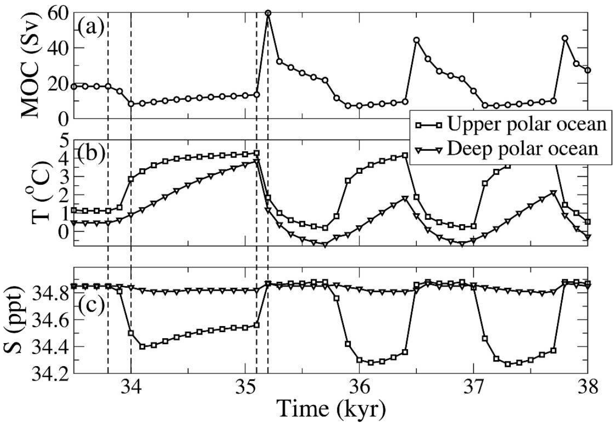

FIG. 2. The OGCM solution for a wind stress strength in the vicinity of the onset of the relaxation oscillations: (a) maximum meridional overturning circulation (Sv), (b) average upper polar ocean temperature (squares) and average deep polar ocean temperature (triangles), and (c) average upper ocean salinity (squares) and average deep ocean salinity (triangles). The polar ocean is defined between 52.5° and 67.5°N. The upper ocean is defined between $z = -1175$ m and the sea surface while the deep ocean is defined between $z = -4500$ m and $z = -1175$ m.

solid linear curve in Fig. 1a indicates the magnitude of the wind stress field given by Eq. (1).

The range of wind amplitude at which the oscillations exist is very different when the wind is decreased from when it is increased. Thus, there is a large regime of wind stress amplitude where both a steady THC state and large relaxation oscillations of the THC can exist. This is the hysteresis with respect to the wind stress amplitude. Unlike the Stommel (1961) hysteresis between steady states, this is a hysteresis between a steady state and an oscillatory regime. Using a three-box model, we demonstrate in the next section the possibility of (i) both salinity and thermally dominant THC states, (ii) two thermally dominant THC states, and (iii) a thermally dominant THC state and an oscillatory regime of THC under the same wind coefficient.

As the wind crosses the threshold that leads to the new regime at 34 kyr, there is a shutdown of the meridional overturning circulation (Figs. 2a and 3, upper panels). This is due to the fact that less low-latitude high salinity water is transferred by the wind-driven circulation to the high latitudes and then cooled there, increasing the high-latitude water density. The weakened wind results in less transport of such salty water and causes the high-latitude surface water to become lighter than the deep water, thus resulting in a stronger stratification and reduced sinking. This results in the "decoupling phase" of the surface from the subsurface waters, as described by Winton (1993). As a result, there is no supply of cold water to the deep ocean and thus the deep ocean temperature increases due to heat diffusion from lower latitudes; accordingly, the deep ocean density decreases. This results in an increase of the THC (Figs. 2b,c) with further increase of the density via the advective THC feedback (Dijkstra 2000). Still, in the very high latitudes, namely, 64.5°–67.5°N, the upper-ocean density is increasing relative to that of the deep ocean due to the effect of the cold atmospheric temperatures. These stages can be seen in the snapshots depicted in Figs. 3e,f,g.

At some point deep ocean water becomes lighter than the very high latitude surface water and enhanced sinking is initiated; this is the "coupled phase" of Winton (1993). Owing to this enhanced sinking, the meridional overturning circulation is restarted at a much larger amplitude and reaches a value of more than 40 Sv in this model (Figs. 3d, 2a). Later, the THC returns to its original rate, when the cycle starts again.

In Fig. 4 we show the sea surface salinity of the upper ocean (averaged over depths 200 to 20 m) at the beginning of the simulation (Fig. 4a) and before the onset of oscillations (Fig. 4b). In both panels the THC is almost the same; however, the salinity gradient is larger when the wind stress is weaker (Fig. 4b), a fact that indicates weaker mixing between the low and high latitudes when the wind stress is weaker. We use this fact in the construction of the box model presented below.

To examine the robustness of the wind-induced THC hysteresis, we repeated the above simulation for a different evaporation minus precipitation field using $f_{e-p} = 0.7$ (Fig. 1b). This results again in the onset of oscillations of the maximum meridional overturning circulation as the wind stress amplitude weakens, and in a hysteresis behavior. There are quantitative differences as the onset of oscillations is for larger wind stress value (Fig. 1b) than with the weaker freshwater forcing (Fig. 1a); this is due to the high-latitude waters that become lighter, even for relatively large wind stress, due to the larger freshwater flux used in this run.

To check the stability of the results presented in Fig. 1 we run two simulations for 20 kyr (Fig. 5) starting from initial conditions associated with stable THC and oscillatory THC (times of 30 and 46 kyr in Fig. 1) with a temporally constant wind stress field. The stable THC (Fig. 5a) as well as the oscillatory THC (fig. 5b) persist throughout the long simulation, indicating that the results of Fig. 1 are not due to transient effects.

As a further test of the robustness of our results, consider the hysteresis plots for different values of the SST restoring times, depicted in Fig. 6. Figure 6a repeats the reference results of Fig. 1a with a restoring time of 24 days. Figure 6b shows that a shorter restoring times of 12 days results in more rapid oscillations, due

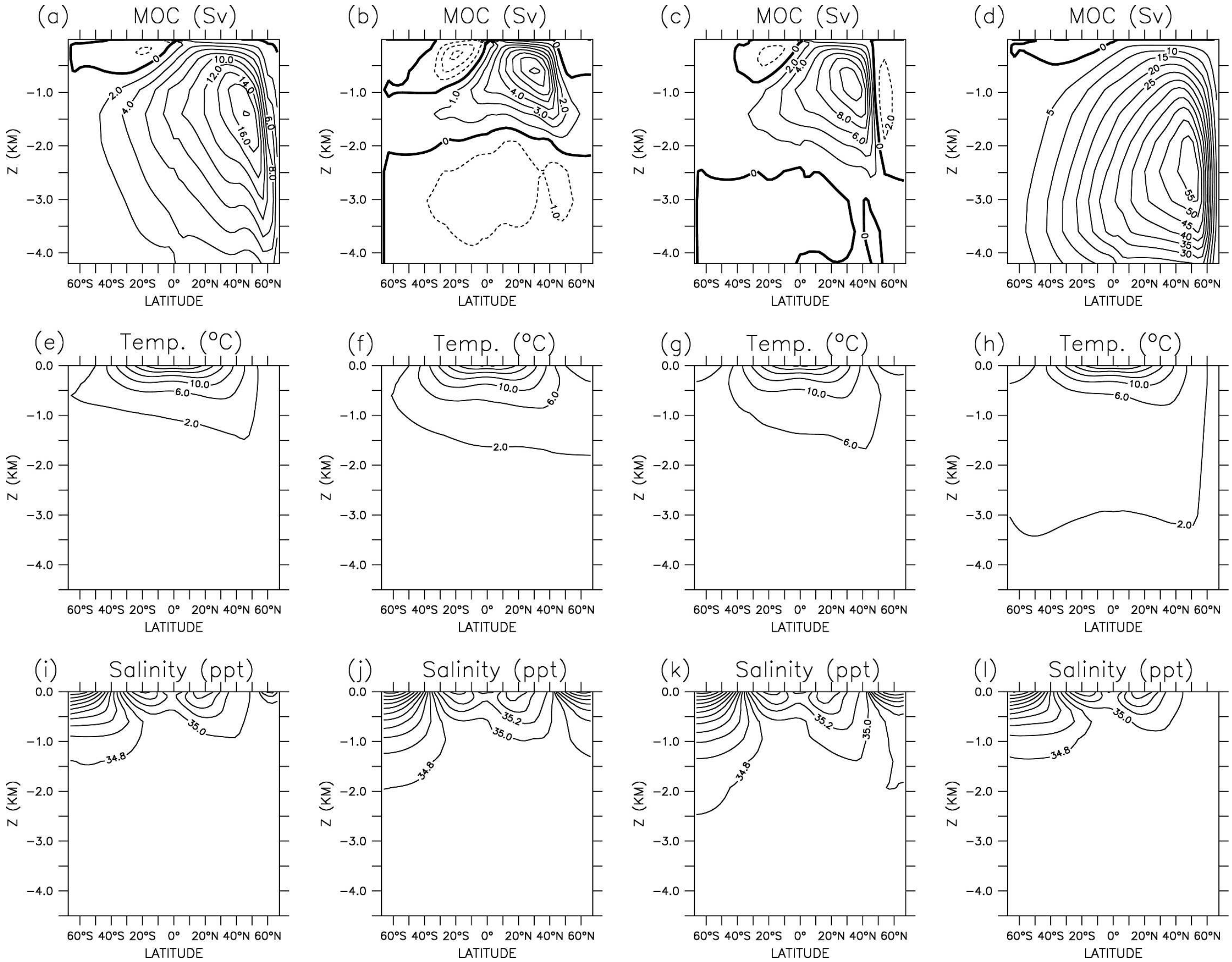

FIG. 3. Snapshots of the OGCM hysteresis simulation during the times indicated by the vertical dashed lines in Fig. 2; the time direction is from left to right: first column corresponds to t = 33.8 kyr, second to t = 34 kyr, third to t = 35.1 kyr, and the fourth to t = 35.2 kyr. These snapshots depict the first relaxation oscillation of the simulation: (top) meridional overturning circulation, (middle) zonally averaged temperature, and (bottom) zonally averaged salinity.

to the faster response to the restoring temperature. With a weaker restoring of 48 days (Fig. 6c), there are no relaxation oscillations because of the stabilizing effect of longer restoring times on the THC (Rahmstorf and Willebrand 1995).

We conclude that the wind-induced hysteresis occurs for several choices of model parameters and does not seem to be an artifact of the simplified surface boundary conditions. It is yet to be shown that the hysteresis also exists with a higher spatial resolution or under a different convective adjustment scheme. We note that the relaxation oscillations seem to be weakly chaotic. As a result, their precise onset time and individual characteristics may be sensitive to various model parameters, although the general model regimes are still robust as shown above.

4. A three-box model of the hysteresis with respect to wind stress

To better understand the hysteresis with respect to the wind stress described in the previous section we construct a simple box model, attempting to couple the mechanisms of Stommel (1961), Winton (1993), and Winton and Sarachik (1993), as well as adding the elements of a varying wind forcing rather than freshwater flux.

The model is a simple generalization of the three-box model of Winton (1993). It consists of two surface boxes, associated with the low and high latitudes of the North Atlantic, and one deep ocean box (Fig. 7). The boxes exchange heat and salt due to mixing processes. The surface boxes are relaxed to specified atmospheric

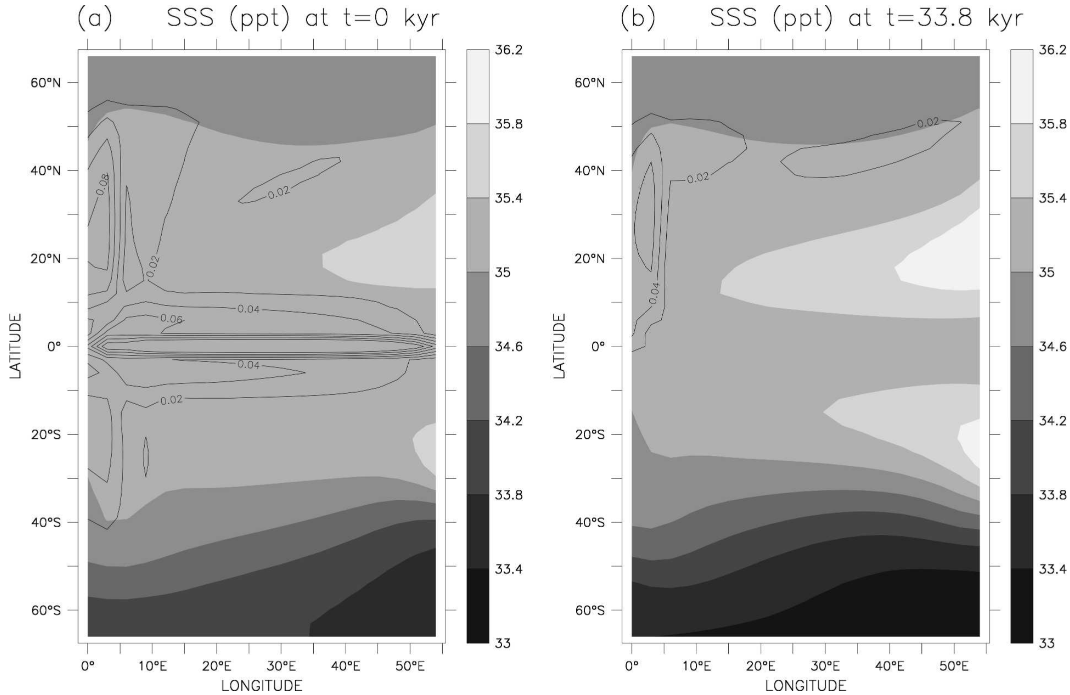

FIG. 4. The average sea surface salinity at (a) the beginning of the simulation and (b) just before the onset of the relaxation oscillations (at t = 33.8 kyr) presented in Fig. 1a. The average is over 200–20-m depth. The contours show the average current magnitude in meters per second.

temperatures. In addition, there is a salinity flux F_s from the high-latitude box to the low-latitude box (corresponding to an atmospheric freshwater flux in the opposite direction) that makes the high-latitude box fresher. To this formulation of Winton (1993), we add a new advection term due to a volume flux q, which represents the THC through all boxes and is determined by

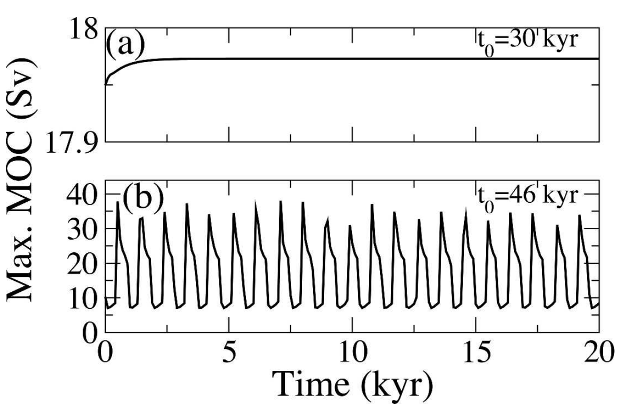

FIG. 5. Maximum meridional overturning circulation vs time under fixed wind stress amplitude (wind stress coefficient of 0.175) starting from initial conditions corresponding to times (a) 30 and (b) 46 kyr of Fig. 1a. Although the boundary conditions are the same, the first initial conditions lead to stable THC while the others lead to strong relaxation oscillations.

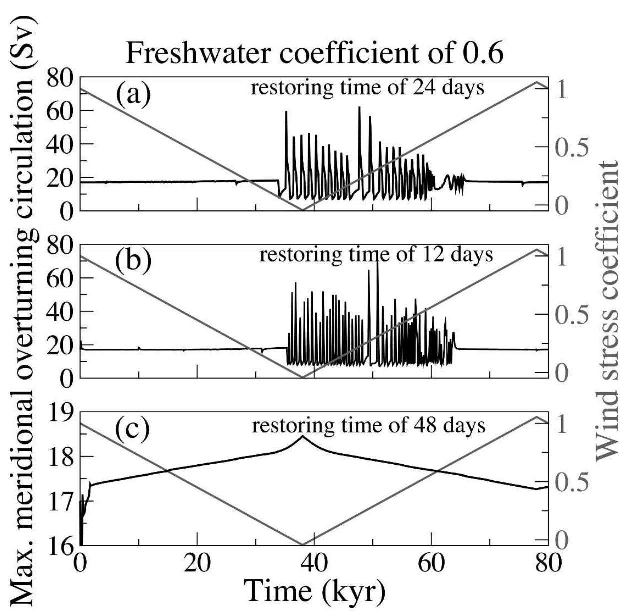

FIG. 6. As in Fig. 1 but for a freshwater coefficient of 0.6, and temperature restoring times of (a) 24 (as in Fig. 1a), (b) 12, and (c) 48 days. The relaxation oscillations are more rapid for stronger restoring (b), while they vanish for weaker restoring (c).

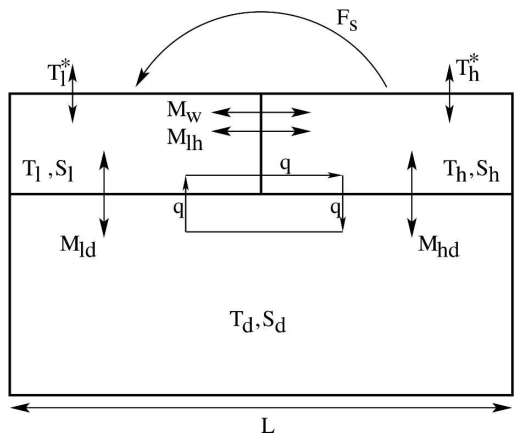

FIG. 7. Three-box model configuration.

the density gradient between the surface boxes (Stommel 1961),

$$q = k(\rho(T_h, S_h) - \rho(T_l, S_l)), \tag{4}$$

where k is a proportionality constant and the equation of state is the one used by Winton (1993),

$$\rho(T, S) = 0.79S - 0.0611T - 0.0055T^2, \tag{5}$$

which is a fit of σ_θ in the temperature range from 0° to 15°. Note that it is necessary to use a nonlinear equation of state to obtain the relaxation oscillations reported by Winton (1993); we also used the UNESCO Equation of State (UNESCO 1983) and obtained similar results to those described below. Unlike the original model of Stommel (1961), we restrict the volume flux to always be positive (i.e., sinking always occurs in the high-latitude box, and the circulation cannot reverse). This is motivated by the fact that ocean general circulation models do not exhibit a reversed THC state with sinking in low latitudes (Bice and Marotzke 2001)—once q as calculated by (4) becomes negative it is set to zero. Another modification we make to Winton's model is the addition of the effect of the wind forcing and wind-driven circulation on the horizontal mixing between the surface boxes. We expect the wind-driven horizontal gyres to mix high-latitude and low-latitude upper-ocean water masses, and therefore crudely represent the effect of the wind-driven circulation as mixing between the low- and high-latitude boxes, with the corresponding mixing coefficient being M_w. Similar treatments of this effect were used in simple models (Longworth et al. 2005; Saltzman 2002; Shaffer and Olsen 2001; Stommel and Rooth 1968), yet the specific form used in these models for the wind-induced mixing term is clearly arbitrary and needs further examination using OGCM simulations.

The salinity and temperature of the low-latitude/high-latitude/deep ocean boxes are annotated by S_l, S_h, S_d, and T_l, T_h, T_d, respectively. The equations that govern the changes in the salinity and temperature of the boxes are

$$\frac{dS_l}{dt} = 2\frac{q + M_{ld}}{hL}(S_d - S_l) + 2\frac{M_{lh} + M_w}{hL}(S_h - S_l) + \frac{F_s}{h}, \tag{6}$$

$$\frac{dS_h}{dt} = 2\frac{M_{hd}}{hL}(S_d - S_h) + 2\frac{q + M_{lh} + M_w}{hL}(S_l - S_h) - \frac{F_s}{h}, \tag{7}$$

$$\frac{dS_d}{dt} = \frac{q + M_{hd}}{HL}(S_h - S_d) + \frac{M_{ld}}{HL}(S_l - S_d), \tag{8}$$

$$\frac{dT_l}{dt} = 2\frac{q + M_{ld}}{hL}(T_d - T_l) + 2\frac{M_{lh} + M_w}{hL}(T_h - T_l) - \gamma(T_l - T_l^*), \tag{9}$$

$$\frac{dT_h}{dt} = 2\frac{M_{hd}}{hL}(T_d - T_h) + 2\frac{q + M_{lh} + M_w}{hL}(T_l - T_h) - \gamma(T_h - T_h^*), \quad \text{and} \tag{10}$$

$$\frac{dT_d}{dt} = \frac{q + M_{hd}}{HL}(T_h - T_d) + \frac{M_{ld}}{HL}(T_l - T_d), \tag{11}$$

where the description and the value of the parameters are given in Table 1. These equations describe the amount of salt and heat entering/leaving the boxes plus the contribution of the surface fluxes. The vertical mixing coefficients are determined according to the stratification; when the density of a surface box is larger than the bottom box density, convection is initiated and the vertical mixing coefficient $M_{l,hd}$ drastically increased:

$$M_{l,hd} = C_{l,h}M_\upsilon, \tag{12}$$

where $C_{l,h}$ increased from 1 to 10 if $\rho(T_{lh}, S_{lh}) > \rho(T_d, S_d)$.

Winton (1993) showed that it is possible to obtain (self-sustained relaxation) oscillations of the salinity and temperature of the boxes for certain values of surface salinity flux F_s. However, our addition of the volume flux q between the low- and high-latitude boxes add the possibility of the Stommel (1961) hysteresis to the model. It is interesting to see how these two different mechanisms interact.

Figure 8 shows the box model's variables for the case in which the wind-induced mixing coefficient M_w decreases linearly over 40 kyr and then increases linearly over another 40-kyr period, as was done using the OGCM (section 3). The volume flux q remains ther-

TABLE 1. The parameters for the three-box model.

Parameter	Short description	Value
W	Zonal dimension	5000 km
H	Depth of the bottom box	4000 m
h	Depth of the surface boxes	100 m
L	Meridional dimension of the bottom box	7000 km
V	Volume of surface boxes	$hLW/2 = 1.75 \times 10^6$ km^3
V_d	Volume of bottom box	$HLW = 1.4 \times 10^8$ km^3
T_l^*	Atmospheric (restoring) temperature of the low-latitude box	15°C
T_h^*	Atmospheric (restoring) temperature of the high-latitude box	0°C
F_s	Surface salinity flux	35 psu $\times$ 2.824 m yr^{-1}, 35 psu $\times$ 4.12 m yr^{-1}
M_v	Vertical background mixing coefficient	$V_d/(400$ yr$) = 11.0984$ Sv
$C_{l,h}$	Low/high-latitude vertical convection coefficient	10
M_{lh}	Horizontal mixing coefficient	$V/(2.5$ yr$) = 22.1969$ Sv, $V/(1.25$ yr$) = 44.3937$ Sv
M_w	(Maximum) wind mixing coefficient	$M_{lh}/5 = 4.439$ Sv, $M_{lh}/20 = 2.22$ Sv
γ	Surface temperature relaxation constant	8×10^{-6}(m s^{-1})$/h = 1/(144.676$ days)
k	Volume flux constant	$0.76V = 42.174$ Sv/(kg m^{-3}), $2V = 110.984$ Sv/(kg m^{-3})

mally dominant for the first half of the simulation, that is, the first 40 kyr (Fig. 8). Just when the wind coefficient is very close to zero, the volume flux q becomes zero [i.e., circulation switches to the salinity-dominant reversed THC state of Stommel (1961) and is being reset to zero]. After approximately 5 kyr, relaxation oscillations very similar to the ones observed by Winton (1993) and in our OGCM experiments are initiated. These oscillations and the hysteresis with respect to the wind stress are very similar to the one obtained by the OGCM and are shown in Figs. 1 and 6. Moreover, there are indications for two thermally dominant states under

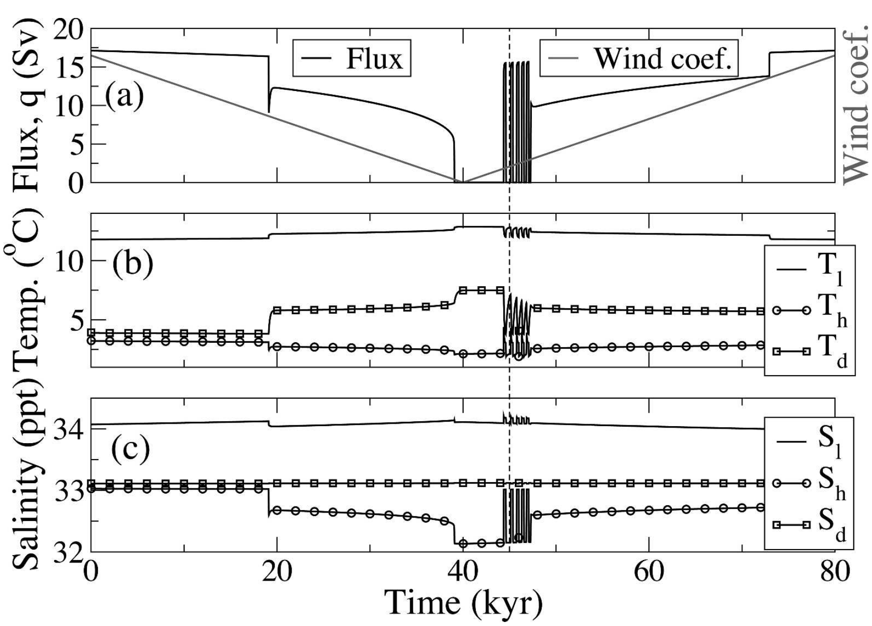

FIG. 8. Three-box model variables as function of time during the hysteresis experiment in which the wind coefficient is decreased very slowly to zero over 40 kyr and then increases again over another 40 kyr. (a) Volume flux q (Sv) in black and wind coefficient in grayscale. (b) The temperature of the boxes. (c) The salinity of the boxes. Note that under the same wind coefficient the model exhibits both a stable thermohaline circulation state with sinking at high latitudes and relaxation oscillations of the thermohaline circulation.

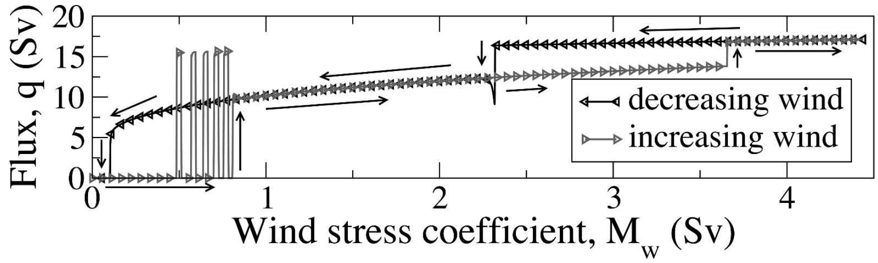

FIG. 9. Thermohaline volume flux q as function of time during the hysteresis run with slowly changing wind-induced mixing coefficient. As in Fig. 8a but with respect to the wind coefficient. The gray areas indicate the wind coefficient for which there are multiple volume flux states: left gray rectangle—thermally dominant state together with shut down and relaxation oscillation state, and right rectangle—two thermally dominant states.

the same wind coefficient (Fig. 9). More precisely, until 20 kyr the volume flux q is approximately 16 Sv when then there is a jump to a lower thermally dominant state with approximately 12 Sv. The transition back to the higher values of volume flux (i.e., during the increasing wind coefficient phase) occurs at a much higher wind amplitude (Fig. 9).

The box temperatures are shown in Fig. 8b and the box salinities in Fig. 8c. The temperature and salinity exhibit similar behavior to that of the volume flux shown in Fig. 8a. It is noticeable that in the oscillation regime (between ~40 and ~60 kyr) the deep box temperature, T_d, decreases linearly similar to the OGCM results (not shown).

We repeat the simulation for different parameter values and obtain similar results, demonstrating again the robustness of the wind-induced THC hysteresis. One example, characterized by a larger regime of oscillations, is seen in Fig. 10. The parameter values are given in Table 1, the second values.

To make sure that the oscillations shown in Figs. 8 and 10 are indeed self-sustained and not a transient effect, we run the model with fixed wind coefficient values starting from the initial conditions in the oscillation regime (indicated by the vertical dashed lines). The results are shown in Fig. 11—the oscillations persist without decaying. From Figs. 8 and 10 it is clear that the frequency of the oscillations becomes greater as the wind coefficient becomes larger. Figure 11a shows the oscillations in a regime that is close to the onset of the oscillations and is thus characterized by weaker frequency oscillations. On the other hand, Fig. 11b shows

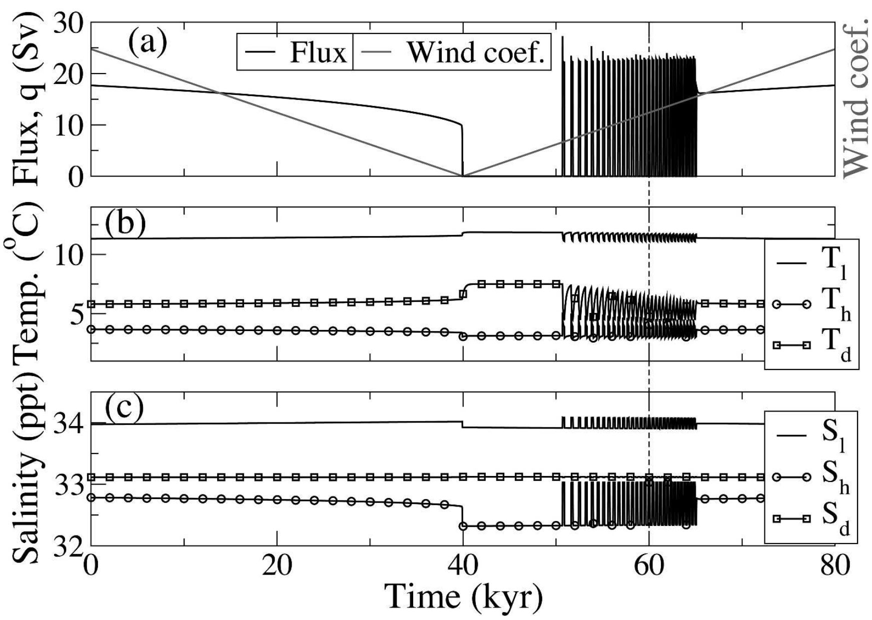

FIG. 10. As in Fig. 8 but for the second choice of parameter in Table 1.

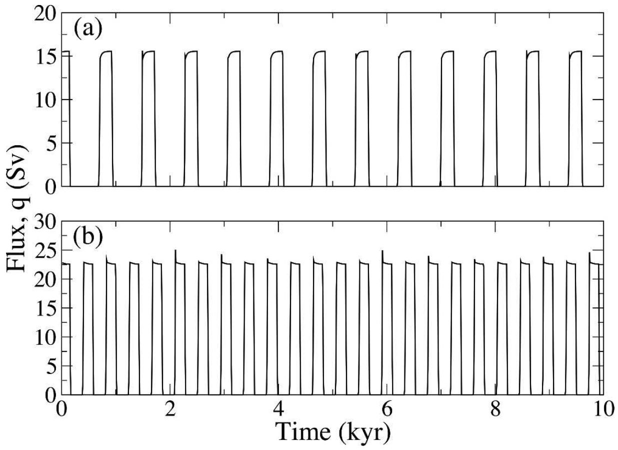

FIG. 11. Oscillations of the box model thermohaline volume q flux with fixed wind coefficient, $M_w = M_{th}/40$, (a) for Fig. 8 configuration (as indicated by the vertical dashed line) and (b) for Fig. 10 configuration (as indicated by the vertical dashed line). Note that the oscillations persist without decay for 10 kyr.

larger frequency oscillations for a wind-induced mixing coefficient that is farther from the onset of oscillations. Such a property is not observed clearly in the OGCM simulations shown in Figs. 1 and 6 although there are indications in that direction.

Our box model formulation assumes that the THC cannot reverse (q must remain positive), following the observation that GCMs, unlike the original Stommel model, often show several possible states of the THC including a collapsed or weakened one, but not a reversed state (Bice and Marotzke 2001). We note that, when allowing for a reversal of the THC as in the original Stommel formulation, we find that the results above for the wind-induced hysteresis, induced oscillatory domain, etc., are very similar to the results described above.

Despite the similarity between the results of the box model and the results of the OGCM there are several caveats regarding the box model simulations. First, the salinity flux that we use in the box model (i.e., $F_s \approx 35$ psu $\times$ 3 m yr^{-1}; see Table 1) is three to four times larger than what can be considered realistic. Second, the OGCM does not show a complete shutdown for several thousands of years before the onset of oscillations, while this is often the case in the box model simulations. Finally, the OGCM shows that oscillations are possible, even when the wind is decreasing; in the box model we observe the oscillations just in the increasing wind phase.

In any case, the close resemblance between the OGCM (Fig. 1) and box model results (Fig. 8) provides a reasonably strong indication that the wind hysteresis in the OGCM indeed involves an interaction of the Stommel (1961) hysteresis with convective relaxation oscillations of Winton (1993), Winton and Sarachik (1993), and with the wind mixing effects—in the box model, an excitation from a zero flux to highly enhanced flux occurs exactly when the flux becomes thermally dominated (see Figs. 9, 10). We therefore feel that the box model has been exceptionally useful in helping to decipher the OGCM results.

5. Summary and discussions

Many studies with a hierarchy of models confirmed the prediction by Stommel (1961) of multiple equilibrium states under the same freshwater flux. However, the stability of the THC with respect to changes in the wind stress amplitude seemed to have received little attention.

Here we report two main results. First, that a decreasing wind stress amplitude may result in the excitation of relaxation oscillations of the meridional overturning circulation, like those reported by Winton (1993) and Winton and Sarachik (1993). Second, there is a clear hysteresis of the dynamical regimes (i.e., the regime of steady-state solution and that of an oscillatory behavior) with respect to the wind stress amplitude. We find that these behaviors can be explained as being due to an interaction of the Stommel (1961) hysteresis with the deep decoupling oscillation mechanism of Winton (1993) and Winton and Sarachik (1993). We also find that the effects of the wind amplitude on the dynamical regimes of the THC are simply due to the horizontal mixing effect of the wind-driven circulation and its effect on salt and heat transfer between the midlatitude and high-latitude upper ocean.

To obtain these results and understanding, we use a hierarchical modeling approach, with the results derived using long integrations of a state-of-the-art OGCM in an idealized geometry, and explained using a simple box model. To understand the OGCM results we constructed a simple three box model by adding a Stommel (1961)–like advection, and a wind-induced horizontal mixing, to the convective THC oscillations model of Winton (1993). The simple box model exhibits similar hysteresis with respect to the wind coefficient as the OGCM. We find this combination to be most useful in understanding what seems to be a novel hysteresis with respect to the wind stress amplitude. It is important to reemphasize, however, that this study was not concerned with an attempt to simulate a realistic parameter regime, but rather the opposite: our objective was to explore the dynamical behavior of the THC and its interaction with the wind forcing for different parameter regimes, which should hopefully contribute to the understanding of THC behavior in more realistic parameter regimes as well.

Relaxation oscillations of the THC (sometimes together with sea ice dynamics) were proposed in the past to have been associated with past climate events like the Heinrich events and Dansgaard–Oeschger oscillations (e.g., Alley et al. 2001; Ganopolski and Rahmstorf 2001, 2002; Kaspi et al. 2004; Paillard and Labeyrie 1994; Timmermann et al. 2002; Winton 1993). One expects the wind to be stronger during glacial times due to the larger equator-to-pole temperature gradient (e.g., Alley 2000). Our results indicate that such a regime is less likely to result in DO-like oscillatory behavior of the THC. However, such a regime may be forced by a THC weakening due to freshwater forcing alone, in spite of the opposing effect of stronger winds.

One of the important lessons from our results, therefore, is the realization that the DO-like regime is determined through a delicate balance between wind and freshwater forcing. We hope that other GCM results will try to examine these conclusions, perhaps in a more realistic geometry and with a more realistic representation of atmospheric feedbacks.

Acknowledgments. We thank Hezi Gildor and Claudia Pasquero for helpful discussions, and Wilbert Weijer and an anonymous reviewer for most constructive comments. This research is supported by the U.S.–Israel Binational Science Foundation. Author ET is supported by the McDonnell Foundation and by the NSF paleoclimate program, Grant ATM-0455470, and YA is supported by the Israeli Center for Complexity Science.

REFERENCES

Adcroft, A., J.-M. Campin, P. Heimbach, C. Hill, and J. Marshall, cited 2002: Mitgcm release 1 manual. MIT/EAPS, Cambridge, MA. [Available online at http://mitgcm.org/sealion/online_documents/manual.html.]

Alley, R. B., 2000: Ice-core evidence of abrupt climate changes. *Proc. Natl. Acad. Sci. USA,* **97,** 1331–1334.

——, S. Anandakrishnan, and P. Jung, 2001: Stochastic resonance in the North Atlantic. *Paleoceanography,* **16,** 190–198.

Bice, K. L., and J. Marotzke, 2001: Numerical evidence against reversed thermohaline circulation in the warm Paleocene/Eocene ocean. *J. Geophys. Res.,* **106,** 11 529–11 542.

Bryan, F., 1986: High latitude salinity effects and interhemispheric thermohaline circulation. *Nature,* **323,** 301–304.

Bryan, K., 1984: Accelerating the convergence to equilibrium of ocean-climate models. *J. Phys. Oceanogr.,* **14,** 666–673.

Cessi, P., 1996: Convective adjustment and thermohaline excitability. *J. Phys. Oceanogr.,* **26,** 481–491.

Dansgaard, W., S. J. Johnsen, H. B. Clausen, D. Dahl-Jensen, N. Gundestrup, C. U. Hammer, and H. Oescger, 1984: North Atlantic climate oscillations revealed by deep Greenland ice cores. *Climate Processes and Climate Sensitivity, Geophys. Monogr.,* Vol. 5, Amer. Geophys. Union, 288–298.

Dijkstra, H. A., 2000: *Nonlinear Physical Oceanography*. Kluwer Academic, 456 pp.

——, and M. J. Molemaker, 1997: Symmetry breaking and overturning oscillations in thermohaline flows: A bifurcation study. *J. Fluid Mech.,* **331,** 169–198.

Edwards, N. R., A. J. Willmott, and P. D. Killworth, 1998: On the role of topography and wind stress on the stability of the thermohaline circulation. *J. Phys. Oceanogr.,* **28,** 756–778.

Ganopolski, A., and S. Rahmstorf, 2001: Rapid changes of glacial climate simulated in a coupled climate model. *Nature,* **409,** 153–158.

——, and ——, 2002: Abrupt glacial climate changes due to stochastic resonance. *Phys. Rev. Lett.,* **88,** 038 501, doi:10.1103/PhysRevLett.88.038501.

Gent, P. R., and J. C. McWilliams, 1990: Isopycnal mixing in ocean circulation models. *J. Phys. Oceanogr.,* **20,** 150–155.

Gildor, H., and E. Tziperman, 2003: Sea-ice switches and abrupt climate change. *Philos. Trans. Roy. Soc. London,* **A361,** 1935–1942.

Gregory, J. M., O. A. Saenko, and A. J. Weaver, 2003: The role of the Atlantic freshwater balance in the hysteresis of the meridional overturning circulation. *Climate Dyn.,* **21,** 707–717.

Griffies, S. M., and E. Tziperman, 1995: A linear thermohaline oscillator driven by stochastic atmospheric forcing. *J. Climate,* **8,** 2440–2453.

Guan, Y. P., and R. X. Huang, 2007: Stommel's box model of thermohaline circulation revisited: The role of mechanical energy supporting mixing and the wind-driven gyration. *J. Phys. Oceanogr.,* in press.

Hall, A., and R. J. Stouffer, 2001: An abrupt climate event in a coupled ocean-atmosphere simulation without external forcing. *Nature,* **409,** 171–174.

Haney, L. R., 1971: Surface boundary condition for ocean circulation models. *J. Phys. Oceanogr.,* **1,** 241–248.

Hasumi, H., and N. Suginohara, 1999: Atlantic deep circulation controlled by heating in the southern ocean. *Geophys. Res. Lett.,* **26,** 1873–1876.

Heinrich, H., 1988: Origin and consequences of cyclic ice rafting in the northeast Atlantic Ocean during the past 130,000 years. *Quat. Res.,* **29,** 142–152.

Houghton, J. T., Y. Ding, D. J. Griggs, M. Noguer, P. J. van der Linden, X. Dai, K. Maskell, and C. A. Johnson, Eds., 2001: *Climate Change 2001: The Scientific Basis*. Cambridge University Press, 881 pp.

Huang, B. Y., P. H. Stone, A. P. Sokolov, and I. V. Kamenkovich, 2003: Ocean heat uptake in transient climate change: Mechanisms and uncertainty due to subgrid-scale eddy mixing. *J. Climate,* **16,** 3344–3356.

Kaspi, Y., 2002: A mechanism for the abrupt warming and simultaneous ice sheet discharge involved in Heinrich events. Master's thesis, Weizmann Institute, Rehovot, Israel, 53 pp.

——, R. Sayag, and E. Tziperman, 2004: A "triple sea-ice state" mechanism for the abrupt warming and synchronous ice sheet collapses during Heinrich events. *Paleoceanography,* **19,** PA3004, doi:10.1029/2004PA001009.

Keeling, R. F., 2002: On the freshwater forcing of the thermohaline circulation in the limit of low diapycnal mixing. *J. Geophys. Res.,* **107,** 3077, doi:10.1029/2000JC000685.

Kohl, A., 2005: Anomalies of meridional overturning: Mechanisms in the North Atlantic. *J. Phys. Oceanogr.,* **35,** 1455–1472.

Lenderink, G., and R. J. Haarsma, 1994: Variability and multiple equilibria of the thermohaline circulation associated with deep-water formation. *J. Phys. Oceanogr.,* **24,** 1480–1493.

Longworth, H., J. Marotzke, and T. F. Stocker, 2005: Ocean gyres and abrupt change in the thermohaline circulation: A conceptual analysis. *J. Climate,* **18,** 2403–2416.

MacMynowski, D. G., and E. Tziperman, 2006: Two-way feedback interaction between the thermohaline and wind-driven circulations. *J. Phys. Oceanogr.,* **36,** 914–929.

Marotzke, J., and J. Willebrand, 1991: Multiple equilibria of the global thermohaline circulation. *J. Phys. Oceanogr.,* **21,** 1372–1385.

——, P. Welander, and J. Willebrand, 1988: Instability and multiple steady states in a meridional-plane model of the thermohaline circulation. *Tellus,* **40A,** 162–172.

Marshall, J., A. Adcroft, C. Hill, L. Perelman, and C. Heisey, 1997a: A finite-volume, incompressible, Navier–Stokes model for studies of the ocean on parallel computers. *J. Geophys. Res.,* **102** (C3), 5753–5766.

——, C. Hill, L. Perelman, and A. Adcroft, 1997b: Hydrostatic, quasi-hydrostatic, and nonhydrostatic ocean modeling. *J. Geophys. Res.,* **102,** 5733–5752.

Nilsson, J., and G. Walin, 2001: Freshwater forcing as a booster of thermohaline circulation. *Tellus,* **53A,** 629–641.

Oka, A., H. Hasumi, and N. Suginohara, 2001: Stabilization of thermohaline circulation by wind-driven and vertical diffusive salt transport. *Climate Dyn.,* **18,** 71–83.

Oliver, K. I. C., A. J. Watson, and D. P. Stevens, 2005: Can limited ocean mixing buffer rapid climate change? *Tellus,* **57A,** 676–690.

Paillard, D., and L. Labeyrie, 1994: Role of the thermohaline circulation in the abrupt warming after Heinrich events. *Nature,* **372,** 162–164.

Pasquero, C., and E. Tziperman, 2004: Effects of a wind driven gyre on thermohaline circulation variability. *J. Phys. Oceanogr.,* **34,** 805–816.

Rahmstorf, S., and J. Willebrand, 1995: The role of the temperature feedback in stabilizing the thermohaline circulation. *J. Phys. Oceanogr.,* **25,** 787–805.

——, and A. Ganopolski, 1999: Simple theoretical model may explain apparent climate instability. *J. Climate,* **12,** 1349–1352.

Redi, M. H., 1982: Oceanic isopycnal mixing by coordinate rotation. *J. Phys. Oceanogr.,* **12,** 1154–1158.

Saltzman, B., 2002: *Dynamical Paleoclimatology: Generalized Theory of Global Climate Change*. Academic Press, 354 pp.

Shaffer, G., and S. M. Olsen, 2001: Sensitivity of the thermohaline circulation and climate to ocean exchanges in a simple coupled model. *Climate Dyn.,* **17,** 433–444.

Stommel, H., 1961: Thermohaline convection with two stable regimes of flow. *Tellus,* **13,** 224–230.

——, and C. Rooth, 1968: On the interaction of gravitational and dynamic forcing in simple circulation models. *Deep-Sea Res.,* **15,** 165–170.

Stouffer, R. J., and Coauthors, 2006: Investigating the causes of the response of the thermohaline circulation to past and future climate changes. *J. Climate,* **19,** 1365–1387.

Timmermann, A., and H. Goosse, 2004: Is the wind stress forcing essential for the meridional overturning circulation? *Geophys. Res. Lett.,* **31,** L04303, doi:10.1029/2003GL018777.

——, H. Gildor, M. Schulz, and E. Tziperman, 2003: Coherent resonant millennial-scale climate oscillations triggered by massive meltwater pulses. *J. Climate,* **16,** 2569–2585.

Toggweiler, J. R., and B. Samuels, 1995: Effect of Drake Passage on the global thermohaline circulation. *Deep-Sea Res.,* **42,** 477–500.

Tsujino, H., and N. Suginohara, 1999: Thermohaline circulation enhanced by wind forcing. *J. Phys. Oceanogr.,* **29,** 1506–1516.

Tziperman, E., 1997: Inherently unstable climate behaviour due to weak thermohaline ocean circulation. *Nature,* **386,** 592–595.

——, J. R. Toggweiler, Y. Feliks, and K. Bryan, 1994: Instability of the thermohaline circulation with respect to mixed boundary conditions: Is it really a problem for realistic models? *J. Phys. Oceanogr.,* **24,** 217–232.

UNESCO, 1983: Algorithms for computations of fundamental properties of seawater. UNESCO Technical Papers in Marine Science 44, 58 pp.

Vallis, G. K., 2000: Large-scale circulation and production of stratification: Effects of wind, geometry, and diffusion. *J. Phys. Oceanogr.,* **30,** 933–954.

Wang, X., P. Stone, and J. Marotzke, 1999: Global thermohaline circulation. Part I: Sensitivity to atmospheric moisture transport. *J. Climate,* **12,** 71–82.

Wang, Z., and L. Mysak, 2006: Glacial abrupt climate changes and Dansgaard-Oeschger oscillations in a coupled climate model. *Paleoceanography,* **21,** PA2001, doi:10.1029/2005PA001238.

Welander, P., 1982: A simple heat–salt oscillator. *Dyn. Atmos. Oceans,* **6,** 233–242.

Winton, M., 1993: Deep decoupling oscillations of the oceanic thermohaline circulation. *Ice in the Climate System,* W. R. Peltier, Ed., NATO ASI Series I: Global Environmental Change, Vol. 12, Springer Verlag, 417–432.

——, and E. S. Sarachik, 1993: Thermohaline oscillation induced by strong steady salinity forcing of ocean general circulation models. *J. Phys. Oceanogr.,* **23,** 1389–1410.

Wunsch, C., 2002: What is the thermohaline circulation? *Science,* **298,** 1179–1181.

——, and R. Ferrari, 2004: Vertical mixing, energy and the general circulation of the oceans. *Annu. Rev. Fluid Mech.,* **36,** 281–314.